Research Article | Vol. 28, No. 21 / 12 October 2020 / Optics Express 31796
Optics EXPRESS

Towards a 20 Gbps multi-user bubble turbulent NOMA UOWC system with green and blue polarization multiplexing

LI ZHANG,[1,4] ZHAOMING WANG,[1,2,4] ZIXIAN WEI,[1,2] CHEN CHEN,[3] GUODAN WEI,[2] H. Y. FU,[1,2,5] AND YUHAN DONG[1,6]

[1]*Shenzhen International Graduate School, Tsinghua University, Shenzhen 518055, China*
[2]*Tsinghua-Berkeley Shenzhen Institute (TBSI), Tsinghua University, Shenzhen 518055, China*
[3]*School of Microelectronics and Communication Engineering, Chongqing University, Chongqing 400044, China*
[4]*These authors contributed equally to this work*
[5]*hyfu@sz.tsinghua.edu.cn*
[6]*dongyuhan@sz.tsinghua.edu.cn*

Abstract: We experimentally demonstrated a high-speed multi-user green and blue laser diode based underwater optical wireless communication (UOWC) system using non-orthogonal multiple access (NOMA) with polarization multiplexing. The system affords eight users with a record sum rate of 18.75 Gbps over 2-m underwater plus 0.5-m free-space channel. The modulation bandwidths of four detachable optical paths with different wavelengths and polarization states all exceed 1.5 GHz. The results suggest that the flexible balance according to both user fairness and overall throughput/sum rate can be achieved via an appropriate power allocation strategy. The joint optimization of driving current and user assignment ensures the feasibility of providing stable high-speed UOWC for multiple users. With the proposed OFDMA-NOMA scheme, user scale expands by twice while the sum rate for single path reaches 3.2 Gbps. Finally, the BER performances of NOMA modality in turbulent underwater environment with air bubbles of different flow rates are also discussed in detail.

1. Introduction

Underwater communications are ushering in rapid development. In summer 2018, Microsoft deployed a packaged data center under the Scottish offshore coast in order to decrease energy consumption caused by device cooling [1]. Meanwhile, the increasing distributed underwater sensor network nowadays requires high-capacity communication to central nodes [2]. Traditional acoustic and radio frequency (RF) communications suffer severely from low-bandwidth and power attenuation, which leads to large transmission delay and limited propagation distance as low as a few centimeters respectively [3]. Therefore, for higher data rate and longer distance, optical communication has been the state of the art to satisfy the requirements [4]. Comparing with optical fiber communication, underwater optical wireless communication (UOWC) is a more flexible and economical approach for high-speed data transmission avoiding expensive C-band lasers and coupling equipment [5–6]. Particularly, the seawater, as a channel, shows a relatively low attenuation characteristic in the wavelength range from 450 to 550 nm [7], which makes mature low-cost green and blue (GB) laser diodes (LDs) and light emitting diodes (LEDs) as favorable light sources for the UOWC. Moreover, different receivers, e. g., silicon photomultiplier [8] and scintillating fiber receiver [9] are utilized to mitigate the turbulence and multi-path effects in a large-scale underwater network.

The research of UOWC is still at its early stage. Researchers have made utmost efforts to enhance the data rate/capacity, transmission distance and scale of UOWC systems. Wang *et al.*

#405417 https://doi.org/10.1364/OE.405417
Journal © 2020 Received 28 Aug 2020; revised 27 Sep 2020; accepted 27 Sep 2020; published 6 Oct 2020

Optics EXPRESS

reported a micro-LED based UOWC system offering data transmission of 933 Mbps on-off keying (OOK) signal over 2.3 m distance with a bit error rate (BER) of 3.75×10^{-3} [10]. Although LEDs can offer a larger coverage probability, the limited bandwidth and power still restrict its application in high-speed and long-distance scenarios. An advanced modulated signal using orthogonal frequency division multiplexing (OFDM) was transmitted to achieve a higher data rate of 4.8 Gbps based on 450 nm LD [11]. Nevertheless, most UOWC systems adopted simplified single-input single-output (SISO) transmission, and multiple-input multiple-output (MIMO) transmission combined with the advanced modulation technique still lacks of experimental demonstration. A 2×2 OFDM system in [12] achieved 33.691 Mbps data rate over 2 m water channel. Another efficient approach to improve channel capacity is wavelength division multiplexing (WDM). Considering illumination effects, different RGB LEDs based UOWC systems have been reported to provide underwater solid-state lighting (SSL) [13–14]. Kong *et al.* further realized underwater communication of 9.51 Gbps in [15]. Combined with polarization multiplexing, the WDM systems show much potential in high-speed free-space transmission [16–17].

On the other hand, multiple access (MA) technology has been proved to be an ideal approach to simultaneously support multiple users and further extend system capacity in free-space optical wireless communication (OWC). One of the advanced MA technologies proved effectively in RF is non-orthogonal multiple access (NOMA). NOMA enables each user to multiplex in the power domain while exploiting entire time slots and frequency bandwidth with different power allocation strategies. For instance, NOMA with fixed power allocation (F-NOMA) is proved to provide a larger sum rate than orthogonal MA, while adaptive/dynamic schemes ensure quality of service (QoS) especially for users with poorer channel conditions [18–19]. Many theoretical works in free-space OWC have demonstrated the capacity superiority of NOMA [20–22]. Whereas only few experiments were conducted to confirm these theoretical analysis [23–25]. Chen *et al.* proposed and experimentally verified a flexible-rate successive interference cancellation (SIC)-free NOMA technique for downlink OWC in [24]. Shi *et al.* reported a real-time OFDM-NOMA OWC system over 1 m free space, which offered two users with total 1.84 Gbps data rate [25]. However, the applications of NOMA in underwater environment are limited. C. Geldard *et al.* evaluated the numerical performance of NOMA system [26] and M. Li *et al.* proposed an emulational model based on MATLAB [27]. Our group demonstrated the capacity superiority of NOMA in underwater turbulent environment [28]. Recently, D. Chen *et al.* reported the first experimental LED-based NOMA system over 1 m distance with rate limited to 117.4 Mbps for only two users [29]. Since most experimental NOMA systems in both free-space and underwater environment are supporting less than three users, large-scale multi-user NOMA system deserves further investigation.

Meanwhile, bubble-induced turbulent flow is another key challenge to UOWC systems. Generally, the impacts of turbulence on the performance of algorithm need necessary consideration when discussing UOWC. L. Chen *et al.* proposed a robust 2×2 MIMO system against the impairments of varied bubble sizes and positions in underwater links [30]. In addition, D. Chen *et al.* studied the influence of the signal intensity fluctuation caused by air bubble, experimentally establishing a best fitting model based on generalized extreme value distribution [31]. Yet the turbulence in NOMA system has not been experimentally testified.

In this paper, to the best of our knowledge, we firstly experimentally demonstrate bicolor GB LDs based eight-user bubble turbulent NOMA UOWC system via polarization multiplexing. The proposed system is capable to support multiple users simultaneously with a record sum rate of 18.75 Gbps over 2-m water tank plus 0.5-m free-space distance. Considering the specific attenuation characteristic of water, GB LDs are chosen as our light sources. Four independent optical paths with each wavelength divided into *s*- and *p*- polarization states are designed for the system. The four paths, each carrying information intended for two users multiplexing in the power domain, have the 3-dB bandwidths of 1.66, 1.54, 1.57 and 1.54 GHz, respectively. For

Optics EXPRESS

each user, the data rate can reach up to 2.34 Gbps, which corresponds to a record sum rate of 18.75 Gbps. Experimentally measured BERs are lower than the forward error correction (FEC) threshold of 3.8×10^{-3}. Moreover, we evaluate power allocation strategy for further performance optimization. The power allocation ratio (PAR) is a core parameter in NOMA since it can decide whether sum rate or fairness is preferred during system optimization. When the PAR is small, users with a superior channel condition will gain better BER performance, which maximizes the overall rate of each link. Conversely, a large PAR can offer a relatively balanced performance for both two users multiplexed in one path, minimizing the influence caused by distinct channel conditions. The proposed OFDMA-NOMA scheme is an effective method to extend maximum user scale by times, and the proof-of-concept system realizes data transmission of 3.2 Gbps for four users. Considering different densities of bubbles, users are still decoded successfully at 2.8 Gbps with an appropriate PAR, which testifies the feasibility of NOMA modality under turbulence. With the demonstration of multiple users and the record rate of 18.75 Gbps for 2.5 m air-water turbulent channel, our NOMA based UOWC system shows high potential of constructing large-scale high-speed communication between underwater base stations, which transmit multiplexed signals for multiple users.

2. Principles of NOMA

NOMA exploits a new domain of signal power so that multiple users could share the same whole bandwidth simultaneously and obtain the maximum data rate. The basic principle of NOMA consists of multi-user superposition coding (SC) at the transmitter (Tx) side and the corresponding decoding method of SIC at the receiver (Rx) side.

The complete coding method is illustrated by simply considering two users, which are denoted as user 1 and user 2 respectively. Different information intended for two users is loaded on two independent pseudo random binary sequences (PRBS) S_1 and S_2 firstly. The generated binary data streams are then modulated into 4-ary quadrature amplitude modulation (QAM) symbols as X_i (i=1, 2), and the traditional SC accomplishes power allocation for users. After power normalization, the corresponding power allocation parameter of NOMA encoding is obtained as

$$a_i = P_i/P \tag{1}$$

and the PAR between two users is defined as

$$\beta = P_2/P_1 = a_2/a_1 \tag{2}$$

The power difference between users determines the degree of decoding difficulty. Without loss of generality, we assume that more power is allocated to user 1, i.e., $\beta < 1$. Consequently, the generated multiplexed signal X is a 16QAM-like signal as shown in Fig. 1(c), of which the expression is given by

$$X = \sqrt{a_1 P}X_1 + \sqrt{a_2 P}X_2 \tag{3}$$

With a properly designed PAR value, performances of two users are compromised so the optimal overall throughput of the system could be achieved. In addition, NOMA operates similarly as a power multiplexer. Some specific operations turn the complex constellation points into real and positive signal which is then intensity modulated into optical beams. Then the received frequency domain 16QAM-like signal at user i is, symmetrically, denoted by Y_i as

$$Y_i = H_i X + N = H_i\left(\sqrt{a_1 P}X_1 + \sqrt{a_2 P}X_2\right) + N, \quad i = 1, 2 \tag{4}$$

where X is the transmitted multiplexed signal, H_i denotes the estimated response of user i, and N represents the noise of the system. Making use of the results from channel estimation, the original

Optics EXPRESS

multiplexed signal Y_i needs further equalization for error correction. Obviously, Y_i contains the superposed effective information intended for two users. Finally, in order to recover original bit sequences, the SIC method separates the QAM signal X_i of user i out of multiplexed signal successively according to the aforementioned power allocation strategy, as shown in Fig. 2(d).

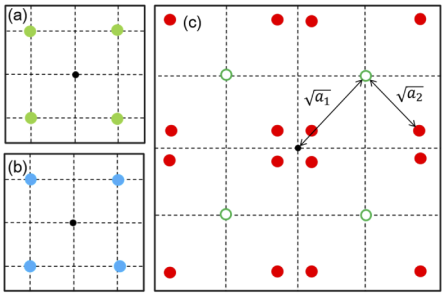

Fig. 1. Constellation diagrams of transmitted signals: (a) QAM signal for user 1, (b) QAM signal for user 2, (c) multiplexed signal of users after power-domain SC.

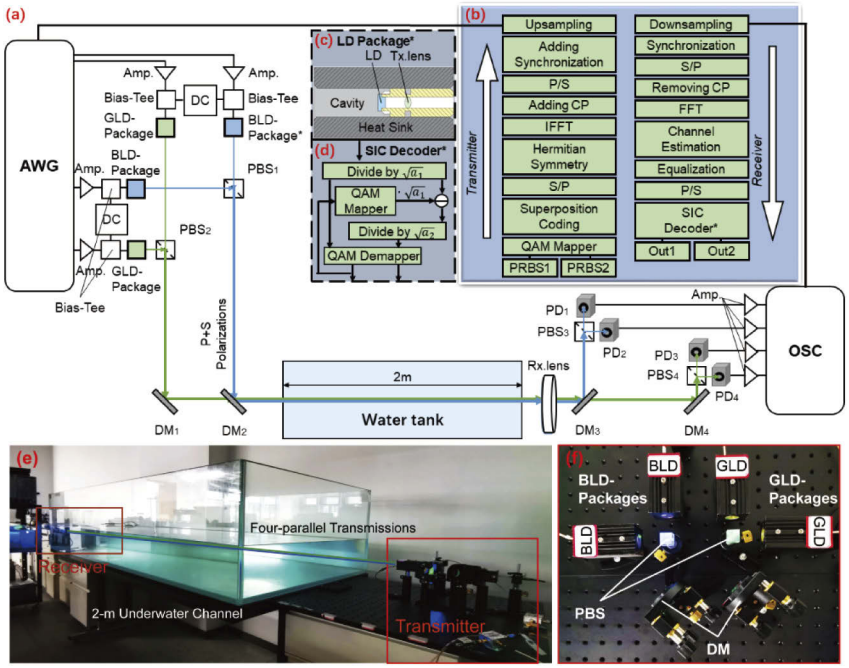

Fig. 2. (a) Experimental setup of bicolor GB LD-based underwater NOMA UOWC system, (b) NOMA signal encoding and decoding processes in MATLAB, (c) section of LD package, (d) schematic diagram of the SIC decoder, (e) image of experimental system, (f) photography of bicolor GB LDs based transmitter. (AWG: arbitrary waveform generator; PBS: polarization beam splitter; DM: dichroic mirror; CF: color filter; OSC: oscilloscope.)

3. Experimental setup

The architecture of the NOMA UOWC system utilizing two sets of bicolor GB LDs with different polarization states is shown in Fig. 2. The transmitted NOMA-OFDM signals are generated in

Optics EXPRESS

MATLAB at the Tx side first and loaded on the experimental optical link to reach Rx side, where the received signals are decoded offline. The corresponding signal processing flows of the Tx and Rx are shown in Fig. 2(b). At the Tx side, arbitrary waveform generators (AWG, AWG7000A, Tektronix) generates NOMA-OFDM signals to two TO packaged bicolor modules consisting of green LDs (PL520) and blue LDs (PL450b). Figure 2(c) shows the side section structure of the LD packages used in the experiment, and each contains a collimating lens, a metallic package and a heat diffuser. The details of the Tx setup are shown in Fig. 2(f). Figure 2(e) shows the image of the overall NOMA UOWC system over 2-m water tank. Our designed system is capable to support eight users simultaneously by assigning each polarized green/blue link for two users respectively. Figure 2(b) shows the flow diagram of signal generator and the data transmission of two users for each polarized link. Firstly, two random binary streams S_1 and S_2 are modulated into 4QAM formats as shown in Figs. 1(a) and (b). Then with the operation of aforementioned SC encoding method, the multiplexed signal of two users presents the 16QAM-like constellation diagram as shown in Fig. 1(c). The inverse fast Fourier transform (IFFT) with Hermitian symmetry is employed to obtain OFDM signal after serial-to-parallel (S/P) conversion. Cyclic prefix (CP) insertion and parallel-to-serial (P/S) conversion are executed successively. After that, the synchronizing sequences are inserted at the front of the serial data.

The generated NOMA-OFDM signal is up-sampled by AWG to implement digital-to-analog conversion (DAC). Before the intensity modulation of bicolor LDs, the signal is amplified first and superimposed with DC by a bias-tee (ZFBT-6GW+, Mini-circuit). The emitted lights with the same wavelength go through the center of polarization beam splitters (PBSs) from two orthogonal orientations, denoted by perpendicular (s) and parallel (p) directions to the plane of incidence respectively, and converge into one beam with two polarization states. In this way, the output green/blue lights are polarization multiplexed by PBS 1 and PBS 2 as shown in Fig. 2. Finally, the polarization multiplexed bicolor GB signal is generated by dichroic mirrors (DMs). After free-space transmission, the light beam goes through a 2-m water tank filled with tap water and further reaches the convex lens at the Rx side. The bicolor GB signal is first separated into green and blue lights by color filters (CF). Symmetrically, different polarization states of blue/green light channels are de-multiplexed by a PBS constituted polarizer. With the concentration of optical lens, the light projected on the center of photodetector module (DET025AL/M, Thorlabs) and transformed into electrical format. Finally, the real-time oscilloscope (RTO, DPO75902SX, Tektronix) collects the NOMA-OFDM signal for offline digital signal processing (DSP) in MATLAB after amplification. Then a serial of operations as shown in Fig. 2(b) are executed to decode the NOMA-OFDM signal and calculate BER values.

To extend our work for even larger scale underwater application scenarios with massive users, we experimentally demonstrate a proof-of-concept OFDMA-NOMA scheme, which is capable to provide four users over a single link. The whole bandwidth is divided equally into low-frequency and high-frequency sub-bands to satisfy OFDMA. Then, two users multiplex in each sub-band by NOMA method. In this kind of OFDMA-NOMA scheme, two users occupying the same sub-band are orthogonal to the other two occupying the adjacent sub-band while being non-orthogonal to each other.

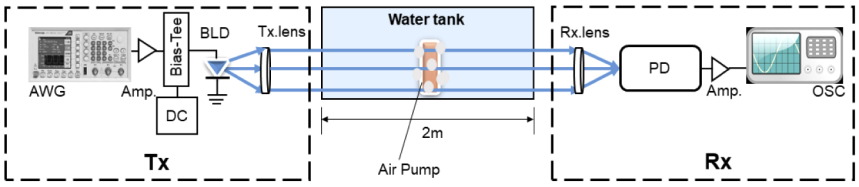

Fig. 3. Experimental setup for bubble-induced underwater NOMA UOWC system based on blue LD.

Optics EXPRESS

Finally, air bubbles are introduced to evaluate the NOMA modality under different intensity fluctuation of bubble-induced turbulence. The foaming area of air pump vertically put in the center of the water tank, as shown in Fig. 3, is 16.5 × 2.5 cm^2. Particularly, the blue LD is chosen here as the light source of the NOMA system. To simulate real conditions, different PAR values are set under varied bubble flow rates to investigate the users' BER performance. The far field distribution of received beam is captured by complementary metal oxide semiconductor (CMOS) camera.

4. Results and discussion

4.1. Characteristic of the UOWC system

The characteristics of the utilized GB LDs including emitting spectrum and optical power, current and voltage (*L-I-V*) are measured and plotted in Fig. 4. The optical spectra in Fig. 4(a) illustrate that the average peak values of GB LDs are 527.8 and 447.6 nm with quite narrow linewidths. Both GB LDs show a good linearity of electrical-to-optical (EO) modulation in Fig. 4(b), where the threshold currents are around 50 and 20 mA respectively. With a relatively low driving current, the blue LD can obtain a higher optical power than the green LD. During the experiment, the output optical powers of the GLDs and BLDs are 30~40 mW and 30~60 mW, which correspond to the biased currents of 130~180 mA and 60~90 mA, respectively.

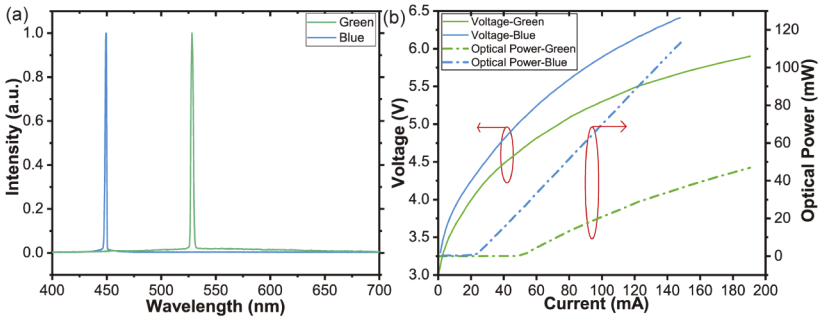

Fig. 4. The measured GB (a) optical spectra and (b) *L-I-V* curves.

For all four links in the designed 2.5-m UOWC system, a vector network analyzer (VNA, N5227A, Agilent) connects, in turn, each one of LDs to the corresponding receiver to measure the normalized responses under different driving currents (voltages) as shown in Fig. 5. The threshold current of green LD could be confirmed in Figs. 5(a) and (b), where the profiles move up and become flat straightly as the driving current exceeds 50 mA. For blue LD, the threshold current in Fig. 5 is also consistent with that shown in Fig. 4. In addition, the related relaxation oscillation peaks are observed at 1.3 GHz when driving current of blue LD exceeds 30 mA. When further increasing driving current up to 40 mA, the measured -3dB bandwidth turns to be stable. The obtained response curves of each path vary with driving current and imply that there is an optimal operating region to derive the best bandwidth performance. Obviously, the record bandwidth values are 1.57, 1.54, 1.54 and 1.66 GHz for link with green-*s*, green-*p*, blue-*s* and blue-*p* light beams. The excellent system bandwidth ensures the capacity to realize high-speed data transmission. Figure 6 illustrates the measured frequency spectra of signals at Rx side. The results show quite smooth and steady channel gain because the signal bandwidth lies within the limit of 3-dB bandwidth. When the sampling rate increases from 2 GHz to 2.5 GHz, high-frequency band deteriorates and fluctuates slightly.

Optics EXPRESS

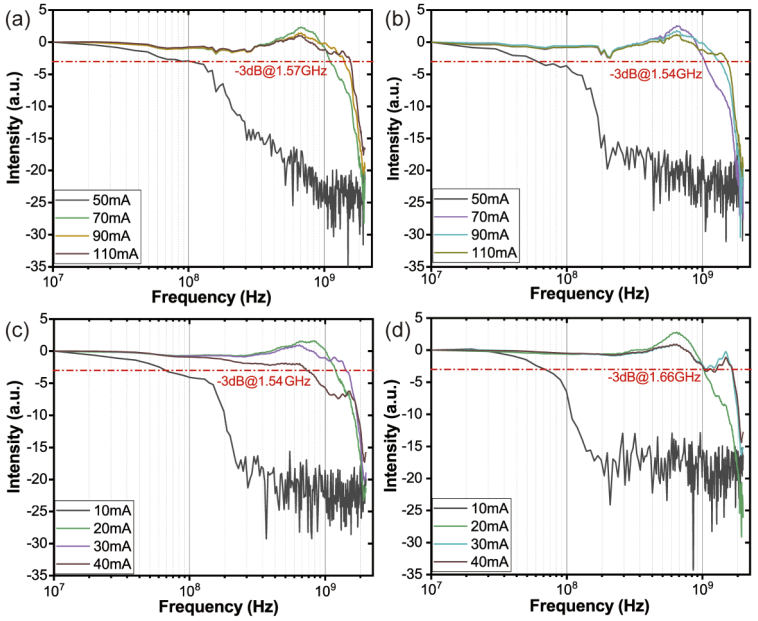

Fig. 5. Measured modulation bandwidths of each link at Rx side: (a) green-*s*, (b) green-*p*, (c) blue-*s* and (d) blue-*p*.

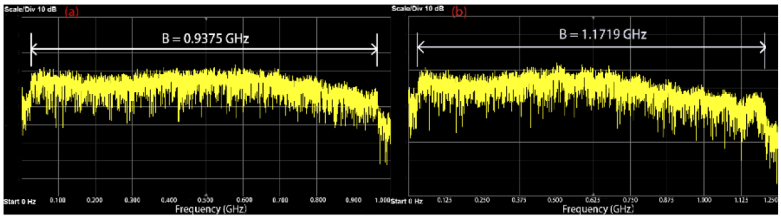

Fig. 6. The frequency spectra for the received signal with sampling rates of (a) 2 GHz and (b) 2.5 GHz.

4.2. BER performance

For system optimization, we evaluate the impacts of driving current of LDs and power allocation strategy of SC encoding jointly. Figure 7(a) plots the calculated BER curves for both two users at blue-*p* polarized link with 60 mA. We assume that $\beta < 1$, which means more power is allocated to user 1. The increasing of PAR narrows the power gap between two users. According to decoding principles that user 1 is always decoded while treating user 2 as interference. The existed error propagation deteriorates the decoding performance of user 2. Hence, in Fig. 7, user 1 always outperformances user 2, and all low-speed points could be decoded error-free. Correspondingly, the BER curves of two users move oppositely as PAR increases, where user 1 and user 2 show a similar performance when PAR reaches 0.40. Further, curves denoting system capacity are plotted in Fig. 7(b). The results suggest that the BER performance and sum rate could be improved by choosing an appropriate PAR value. The power allocation strategy is capable to regulate the balance between user fairness and overall capacity.

Then with the fixed PAR of 0.30, we evaluate the effects of driving current to the decoding performance of users over blue-*p* and green-*p* polarized paths respectively. As shown in Fig. 7(c) and (d), for green LD with data rate lower than 2.25 Gbps, the optimal value of driving current is

Optics EXPRESS

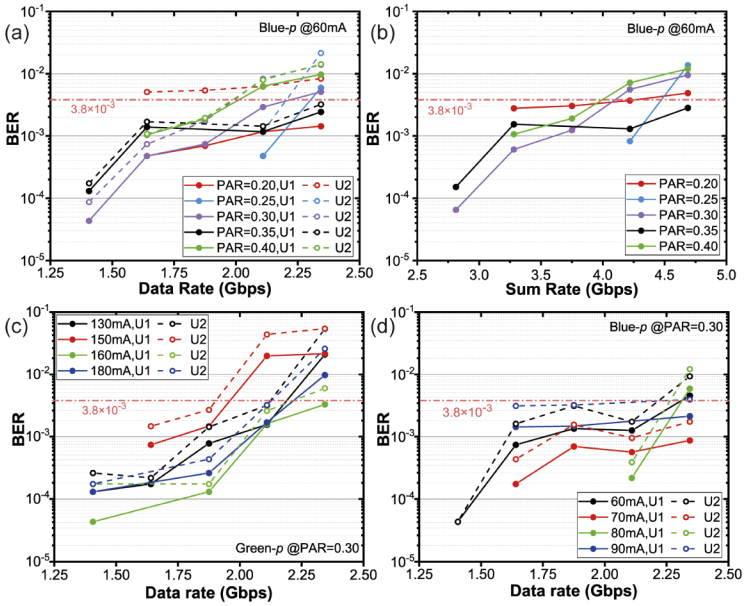

Fig. 7. The BER performance of (a) user 1 and user 2, (b) sum rate on the link blue-*p* at 60 mA with different PAR values; the BER curves of users over (c) green-*p* and (d) blue-*p* links, respectively, under varied driving currents with PAR fixed at 0.30.

160 mA, while blue LD at 70 mA outperforms others. The fluctuation of BER performances originate from limited linear range of *L-I* characteristic and channel responses under different currents. The regular constellation diagrams shown in Fig. 8 attest good decoding performance of the SIC method. Two rows of constellation diagrams indicate different signals respectively at the sampling rate of 1.5 GHz and 2.5 GHz on the link green-*s* with PAR of 0.30 and current of 110 mA. Figure 8(a) and (d) denote the obtained 16QAM-like QAM-NOMA signal after equalization, which are consistent with Fig. 1(c) at the transmitter. Since the signal of user 1 is directly decoded by scaling the multiplexed signal as given in Eq. (4), the constellation in Fig. 8(b) presents a 16QAM-like diagram similar to Fig. 8(a).

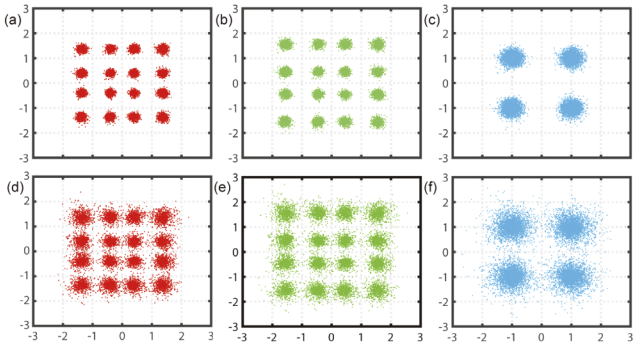

Fig. 8. The constellation diagrams for the received multiplexed signal, the decoded signal for user 1 and user 2 at the sampling rate of 1.5 GHz ((a), (b), (c)) and 2.5 GHz ((d), (e), (f)).

For user 2, the QAM signal, corresponding to Fig. 1(b), is extracted after removing successive interference. Obviously, the constellation points get blurred and dispersive as the increasing

Optics EXPRESS

of sampling rate, which corresponds to a relatively poor decoding performance. From the aforementioned conclusion, both driving current and PAR together determine the performance of the system. By varying PAR values from 0.20 to 0.40 and setting several different currents, we have obtained the highest data rate up to 4.685 Gbps for each path with both two users satisfying the FEC criteria. Then the sum rate of our demonstrated 2.5 m NOMA GB polarization multiplexing UOWC system reaches up to 18.75 Gbps with corresponding parameters listed in Tab. 1. The difference between channels results from characteristics of LDs, optical links and experimental operations. Both user 1 and user 2 can decode multiplexed signal successfully with BER lower than 3.8×10^{-3}, which shows the potential for an even higher rate.

Table 1. Parameters of realizing the optimal user performance

Link	Data Rate (Gbps)	PAR	Current (mA)	BER	
				User 1	User 2
Green-*s*	4.6875	0.3	110	2.17×10^{-3}	3.48×10^{-3}
Green-*p*	4.6875	0.2	180	3.04×10^{-4}	3.17×10^{-3}
Blue-*s*	4.6875	0.2	60	4.35×10^{-4}	3.65×10^{-3}
Blue-*p*	4.6875	0.3	70	8.70×10^{-4}	1.74×10^{-3}

4.3. BER performance of OFDMA-NOMA scheme

Based on the obtained results, the sum rate of four users reaches up to 3.2 Gbps and corresponding BER performance is shown in Fig. 9, where user 1 and user 2 locate at the low-frequency band while user 3 and user 4 locate at the high-frequency band. The orthogonality ensures user decoding to be conducted simultaneously without extra delay comparing to NOMA scheme. User 1 and user 2 always outperform user 3 and user 4 because of higher channel gain of corresponding frequency band. However, the channel response deteriorates with increasing sampling rates of user 3 and user 4, which impairs the sum rate. The PAR of NOMA is fixed as 0.35 so the user 1 and user 3 can have a better decoding performance in the corresponding group, which is consistent with the aforementioned discussion. In this way, this OFDMA-NOMA scheme is capable to support 16 users with potential sum rate above 10 Gbps.

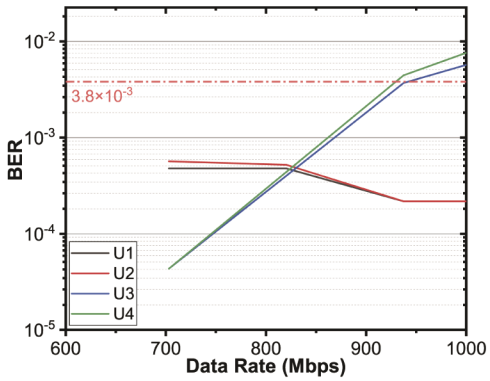

Fig. 9. BER performance for the proof-of-concept OFDMA-NOMA underwater system.

4.4. BER performance of air-bubbles scheme

To investigate the effects of PAR values in mitigating the turbulence-induced interference, BER curves are measured at a data rate of 2.8 Gbps with four different flow rates, i. e. 1, 6, 11 and 16

Optics EXPRESS

L·min^{-1}. The photographs of air bubbles and CMOS images of received light beam are illustrated in Fig. 10. As the increasing of flow rate, the received far field intensity shown on the second line of Fig. 10 fluctuates fiercely while its peak value declining. A specific PAR generates a shaped 16QAM signal while a specific flow rate leads to a time-varying channel response. Hence, each condition is measured five times and then averaged to represent BER performance. Obviously, decoding performance would deteriorate with ascending flow rates in Fig. 11. Users obtain an optimal result with PAR fixed at 0.35. A reasonable explanation is that the optimal PAR relies on mean channel response. The results manifest that an appropriate PAR in NOMA can mitigate deterioration caused by bubble-induced turbulence.

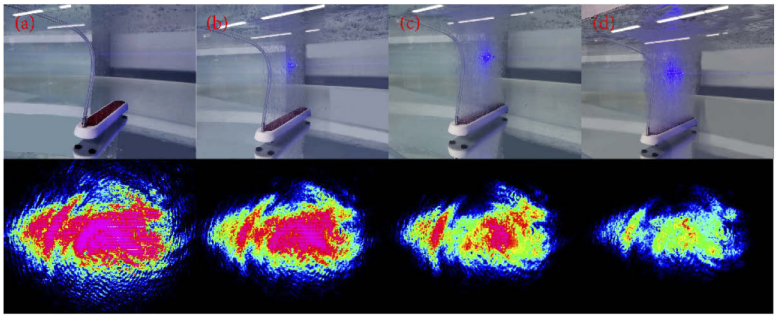

Fig. 10. Photographs and far field images of lights captured under different bubble flow rates of (a) 1 L·min^{-1}, (b) 6 L·min^{-1}, (c) 11 L·min^{-1}, and (d) 16 L·min^{-1}.

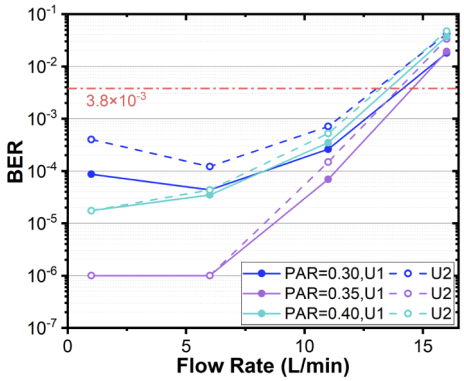

Fig. 11. BER performance with different air-bubble flow rates and PAR values.

5. Conclusion

In this work, we experimentally demonstrate a multi-user NOMA UOWC system with GB polarization multiplexing over 2-m water tank plus 0.5-m free space channel. The highest 3-dB bandwidth for the designed optical links reaches up to 1.66 GHz. Then the record sum rate of 18.75 Gbps is achieved while affording total eight users with all corresponding BER values below the FEC criteria of 3.8×10^{-3}. We also evaluate the impacts of both driving current and power allocation strategy on users' BER performance. The obtained results suggest that parameter optimization could improve the overall system performance and be flexible to different scenarios where users have distinct conditions. Different choices of PAR are capable to make a trade-off between user fairness and overall sum rate. By combining the NOMA with OFDMA, we set up a

Optics EXPRESS

proof-of-concept OFDMA-NOMA system to provide four users over a single link, which enlarges the scale by twice and shows a potential to scenarios with massive users. Furthermore, we take air bubbles of different flow rates into considerations, and results illustrate that adjusting PAR could relatively mitigate the interference induced by turbulence in our NOMA modality. The demonstrated NOMA UOWC system provides a choice for further implementation of large-scale high-speed multi-user communication in future turbulent UOWC networks, e. g. water surface station to central node of distributed sensors.

Funding

Science, Technology and Innovation Commission of Shenzhen Municipality (JCYJ20170818094001391, JCYJ20180507183815699); Tsinghua-Berkeley Shenzhen Institute (TBSI) Faculty Start-up Fund; Shenzhen Fundamental Research Project (JCYJ20170817161720819); Overseas Research Cooperation Fund of Tsinghua Shenzhen International Graduate School (HW2018003).

Disclosures

The authors declare no conflicts of interest.

References

1. Microsoft, "A research project to determine the feasibility of subsea datacenters powered by offshore renewable energy," https://natick.research.microsoft.com/
2. J. Heidemann, M. Stojanovic, and M. Zorzi, "Underwater sensor networks: applications, advances and challenges," Phil. Trans. R. Soc. A. **370**(1958), 158–175 (2012).
3. E. M. Sozer, M. Stojanovic, and J. G. Proakis, "Underwater acoustic networks," IEEE J. Ocean. Eng. **25**(1), 72–83 (2000).
4. Z. Zeng, H. Zhang, Y. Dong, and J. Cheng, "A survey of underwater wireless optical communication," IEEE Commun. Surv. Tutorials **19**(1), 204–238 (2017).
5. A. Li, W. Peng, Y. Cui, and Y. Bai, "80-GBd probabilistic shaped 256QAM transmission over 560-km SSMF enabled by dual-virtual-carrier assisted Kramers-Kronig detection," in *Optical Fiber Communication Conference (OFC) 2020*, paper M3J.8 (2020).
6. O. Ergul, E. Dinc, and O. B. Akan, "Communicate to illuminate: State-of-the-art and research challenges for visible light communications," Phys. Commun. **17**, 72–85 (2015).
7. S. Q. Duntley, "Light in the sea," J. Opt. Soc. Am. **53**(2), 214–233 (1963).
8. M. Khalighi, T. Hamza, S. Bourennane, P. Léon, and J. Opderbecke, "Underwater wireless optical communications using silicon photo-multipliers," IEEE Photonics J. **9**(4), 1–10 (2017).
9. C. H. Kang, A. Trichili, O. Alkhazragi, H. Zhang, R. C. Subedi, Y. Guo, S. Mitra, C. Shen, I. S. Roqan, T. K. Ng, M. Alouini, and B. S. Ooi, "Ultraviolet-to-blue color-converting scintillating-fibers photoreceiver for 375-nm laser-based underwater wireless optical communication," Opt. Express **27**(21), 30450–30461 (2019).
10. P. Wang, H. Chen, X. Liu, S. Yi, X. Zhou, E. Gu, K. Huang, L. Zheng, R. Liu, X. Cui, and P. Tian, "A GaN micro-LED based underwater wireless optical communication subjected to sea salt, Maalox and Chlorophyll," *2018 15th China International Forum on Solid State Lighting: International Forum on Wide Bandgap Semiconductors China* (SSLChina: IFWS), Shenzhen, 1–3 (2018).
11. H. M. Oubei, J. R. Duran, B. Janjua, H. Y. Wang, C. T. Tsai, Y. C. Chi, T. K. Ng, H. C. Kuo, J. He, M. S. Alouini, G. R. Lin, and B. S. Ooi, "4.8 Gbit/s 16-QAM-OFDM transmission based on compact 450-nm laser for underwater wireless optical communication," Opt. Express **23**(18), 23302–23309 (2015).
12. Y. Song, W. Lu, B. Sun, Y. Hong, F. Qu, J. Han, W. Zhang, and J. Xu, "Experimental demonstration of MIMO-OFDM underwater wireless optical communication," Opt. Commun. **403**, 205–210 (2017).
13. X. Liu, S. Yi, X. Zhou, S. Zhang, Z. Fang, Z. Qiu, L. Hu, C. Cong, L. Zheng, R. Liu, and P. Tian, "Laser-based white-light source for high-speed underwater wireless optical communication and high-efficiency underwater solid-state lighting," Opt. Express **26**(15), 19259–19274 (2018).
14. X. Liu, S. Yi, Y. Huang, H. Chen, Z. Qian, R. Lin, X. Zhou, G. Zhou, X. Zhou, S. Zhang, X. Cui, L. Cheng, R. Liu, and P. Tian, "Underwater wireless optical communication and underwater solid-state lighting based on RGB laser diodes mixed white-light," *2018 15th China International Forum on Solid State Lighting: International Forum on Wide Bandgap Semiconductors China* (SSLChina: IFWS), 1–3 (2018).
15. M. Kong, W. Lv, T. Ali, R. Sarwar, C. Yu, Y. Qiu, F. Qu, Z. Xu, J. Han, and J. Xu, "10-m 9.51-Gb/s RGB laser diodes-based WDM underwater wireless optical communication," Opt. Express **25**(17), 20829–20834 (2017).
16. I. C. Lu, C. H. Lai, C. H. Yeh, and J. Chen, "6.36 Gbit/s RGB LED-based WDM MIMO visible light communication system employing OFDM modulation," *2017 Optical Fiber Communications Conference and Exhibition (OFC)*, Paper W2A39.

Optics EXPRESS

17. L. Wei, C. Chow, G. H. Chen, Y. Liu, C. H. Yeh, and C. W. Hsu, "Tricolor visible-light laser diodes based visible light communication operated at 40.665 Gbit/s and 2 m free-space transmission," Opt. Express **27**(18), 25072–25077 (2019).
18. Z. Ding, P. Fan, and H. Poor, "Impact of user pairing on 5G nonorthogonal multiple-access downlink transmissions," IEEE Trans. Veh. Technol. **65**(8), 6010–6023 (2016).
19. Z. Yang, P. Xu, J. Hussein, and P. Fan, "Adaptive power allocation for uplink non-orthogonal multiple access with semi-grant-free transmission," *IEEE Wireless Communications Letters*, 1 (2020).
20. R. C. Kizilirmak, C. R. Rowell, and M. Uysal, "Non-orthogonal multiple access (NOMA) for indoor visible light communications," in *Proc. of IWOW*, 98–101 (2015).
21. H. Marshoud, P. C. Sofotasios, S. Muhaidat, G. Karagiannidis, and B. S. Sharif, "On the performance of visible light communication systems with non-orthogonal multiple access," IEEE Trans. Wireless Commun. **16**(10), 6350–6364 (2017).
22. L. Yin, W. O. Popoola, X. Wu, and H. Haas, "Performance evaluation of non-orthogonal multiple access in visible light communication," IEEE Trans. Commun. **64**(12), 5162–5175 (2016).
23. B. Lin, W. Ye, X. Tang, and Z. Ghassemlooy, "Experimental demonstration of bidirectional NOMA-OFDMA visible light communications," Opt. Express **25**(4), 4348–4355 (2017).
24. C. Chen, W.-D. Zhong, H. Yang, P. Du, and Y. Yang, "Flexible-rate SIC-free NOMA for downlink VLC based on constellation partitioning coding," IEEE Wireless Commun. Lett. **8**(2), 568–571 (2019).
25. J. Shi, Y. Hong, R. Deng, J. He, L. Chen, and G. Chang, "Demonstration of real-time software reconfigurable dynamic power-and-subcarrier allocation scheme for OFDM-NOMA-based multi-user visible light communications," J. Lightwave Technol. **37**(17), 4401–4409 (2019).
26. C. Geldard, J. Thompson, and W. O. Popoola, "A study of non-orthogonal multiple access in underwater visible light communication systems," in *2018 IEEE 87th Vehicular Technology Conference (VTC Spring)*, 120–124 (2018).
27. M. Li and Y. Xiang, "A photon counting underwater NOMA wireless optical communication system," in *2019 7th International Conference on Information, Communication and Networks (ICICN)*, 120–124 (2019).
28. L. Zhang, Y. Chen, K. Zhang, J. Quan, Z. Li, and Y. Dong, "On performance of multiuser underwater wireless optical communication systems," *2020 International Conference on Computing, Networking and Communications (ICNC)*, 1042–1046 (2020).
29. D. Chen, W. Yue, J. Jin, H. Lu, and J. Wang, "An experimental study of NOMA in underwater visible light communication system," Opt. Commun. **475**, 126199 (2020).
30. L. Chen, Y. Shao, and R. Deng, "Robust UOWC systems against bubble-induced impairments via transmit/receive diversities," Chin. Opt. Lett. **17**(10), 100006 (2019).
31. D. Chen, J. Wang, S. Li, and Z. Xu, "Effects of air bubbles on underwater optical wireless communication," Chin. Opt. Lett. **17**(10), 100008 (2019).